An Integral Active Contour Model for Convex Hull and Boundary Extraction

Nikolay Metodiev Sirakov[1] and Karthik Ushkala[2]

[1] Dept. of Mathematics
[1,2] Dept. of Computer Science,
Texas A&M University-Commerce, Commerce-Tx, 75429
Tel.: 9038865943, 9032178843, Fax: 9038865945
Nikolay_Sirakov@tamu-commerce.edu, kushkala@leo.tamu-commerce.edu

Abstract. This paper presents a new deformable model capable of segmenting images with multiple complex objects and deep concavities. The method integrates a shell algorithm, an active contour model and two active convex hull models. The shell algorithm automatically inscribes every image object into a single convex curve. Every curve is evolved to the boundary's vicinity by the exact solution of a specific form of the heat equation. Further, if re-parametrization is applied at every time step of the evolution the active contour will converge to deep concavities. But if distance function minimization or line equation is used to stop the evolution, the active contour will define the convex hull of the object. Set of experiments are performed to validate the theory. The contributions, the advantages and bottlenecks of the model are underlined at the end by a comparison against other methods in the field.

1 Introduction

In recent years new scientific fields emerged such as image semantics extraction and events discovery in images and video. But the very first problem to solve, in order to approach the above sophisticated tasks, is the problem of image segmentation.

Different kinds of techniques are employed for segmentation but some of the most successful in terms of connectivity detection and preservation are the so called active contour models. They could be sub divided to regions [2,3] or boundary detection methods [1,4,5,6,7,11,12]. Another classification of the active contour models may be done on the base of the mathematical method(s) lying behind the algorithm. Thus, there are models based on minimization of functionals [5,12], level set [2,8,10,11], the approximate solution of partial differential equation [1,8,4,9,17], and algebraic structures [13].

The present paper develops a new Integral Active Contour Model (IACH) composed by the shell algorithm, a new active contour model and two new active convex hull models. The shell algorithm[1,14] is used to segment an image with multiple objects, inscribing every object into a convex closed curve. Further every curve is evolved toward the vicinity of the boundary. The evolution is guided

G. Bebis et al. (Eds.): ISVC 2009, Part II, LNCS 5876, pp. 1031–1040, 2009.

by the exact solution of the Active Convex Hull Model (ACHM) [1], which is a specific form of the geometric heat differential equation. From the position of boundary vicinity the IACM may determine: the objects boundary; convex hull; or deep concavities [16]. An arc length re-parametrization [1,14,15,17] is used to facilitate the contour's evolution to the boundary of deep and complex concavities.

A minimization of a distance function and line equation are applied along with the evolution equation to develop two new active convex hull models. The distance function measures the Euclidian distance between the initial position of every active contour point and its location in the vicinity of the boundary.

The rest of the paper is organized as follows: Section 2 develops new Active Contour model on the Exact Solution (ACES) of the ACHM [1] and its extension to objects with deep concavities. Section 3 presents the two new active convex hull models, whereas Section 4 develops the mathematical description of the shell algorithm in the light of the ACES model. The theory is validated by experiments with synthetic and medical images (the x-ray is provided by the Hunt Regional Community Hospital) given across sections 2-4. Section 5 presents more experimental results obtained from images containing craft objects. A PC with Core Duo CPU 2.16GHz, 2.16GHz and 2GB of RAM was used to carry the experiments. Section 6 provides a discussion on the advantages and disadvantages of the present work. A comparison with existing methods underlines the contributions of the IACM.

2 The Active Contour Model on the Exact Solution

The present section develops a new Active Contour model using the Exact Solution (ACES) of the ACHM [1] presented with the following equation:

$$\frac{\partial \psi}{\partial t} = Pk\overrightarrow{N} - |ds|\mathbf{T}, \tag{1}$$

where $\psi = \psi(x(s,t), y(s,t))$ is a parametric curve. In the last expression s parameterizes a particular curve, whereas t parameterizes the family of curves. $\mathbf{T}$ denotes the tangent vector, $\overrightarrow{N}$ the normal one, k is the curvature and P is a penalty function such that:

$$P = \begin{cases} 0 & \text{if } \varepsilon_2 > \frac{\partial f(x,y)}{\partial t} > \varepsilon_1, \\ 1 & \text{otherwise} \end{cases}$$

where $\varepsilon_1, \varepsilon_2$ are thresholds, $f(x,y)$ is the image function.

Thus, if the exact solution of Eq(1) is sought in the form of a separable function $\psi(s,t) = w(t)u(s)$ then this solution is determined as a parametric curve ψ:

$$\psi(s,t) = \exp^{\left(s\frac{|ds|}{2} - \lambda^2 t\right)}[C_1 \cos\left(\frac{s}{2}\sqrt{4\lambda^2 - |ds|^2}\right) + C_2 \sin\left(\frac{s}{2}\sqrt{4\lambda^2 - |ds|^2}\right)], \tag{2}$$

where $\frac{\omega_t}{\omega} = -\lambda^2$ and $|ds|$ is the length of the chord of the arc segment. Substitute $\lambda = |ds|$ in Eq(2) and rewrite it in a vector form:

$$r(s,t) = xi + yj = \exp^{\left(s\frac{|ds|}{2} - |ds|^2 t\right)} [C_1 \cos\left(c\frac{|ds|}{2}s\sqrt{3}\right) i + C_2 \sin\left(c\frac{|ds|}{2}s\sqrt{3}\right) j]. \quad (3)$$

If c varies from 1 to 1000 the curve described by Eq(3) will change its shape from a spiral to a circle, for $s \in [0, 2.309\frac{\pi}{c|ds|}]$. For such s and $t \in [0, \infty]$ the ACES model, is defined by Eq(3) and satisfies the following initial and object boundary conditions. The initial condition is:

$$r(s,t)|_{t=0.001,\, \frac{|ds|}{2}=a, C_1=C_2=R, c=1000} = R\exp^{\left(sa-4a^2 0.001\right)} [cos\left(1000\sqrt{3}as\right), \sin\left(1000\sqrt{3}as\right)]. \quad (4)$$

In Eq(4) $R = \frac{1}{2}\sqrt{nr^2 + nc^2}$, nr - shows the number of rows in the image, nc - is the number of columns. Recall that $f(x,y)$ denotes the image function, where:

$$x(s,t) = R\exp^{(sa-4a^2t)}\, cos(1000\sqrt{3}as), y(s,t) = R\exp^{(sa-4a^2t)}\, sin(1000\sqrt{3}as),$$

for $(x,y) \in D_f$ (the image domain) and $(x,y) \in r(x,y)$. Now the following object boundary condition is formulated:

$$r(s^*,t^*) = r(s^*,t^* + \partial t) \text{ if } \varepsilon_2 > \frac{\partial f(s^*,t)}{\partial t} > \varepsilon_1 \text{ for } s = s^* \text{ and } t^* > 0.001, \quad (5)$$

and $r(s^*,t^*) \neq r(s^*,t^* + \partial t)$ if the above double inequality is not satisfied.

ACES model presented by Eqs(3), (4) and (5) was coded in Java. The thresholds $\varepsilon_1, \varepsilon_2$ and Δt (the discrete form of ∂t) are selected by the user. An experiment was performed using a CT section of brain with a size 256x256 (see Fig 1(a)). In Fig 1(b)the initial contour inscribes the entire image and evolves towards the object boundary. The software took 0.016 sec, to extract the boundary shown in Fig 1(c).

The ACES model evolves the active contour toward the objects boundary, but experiences difficulties to progress into deep concavity (Figs 2(a),3(a)). To

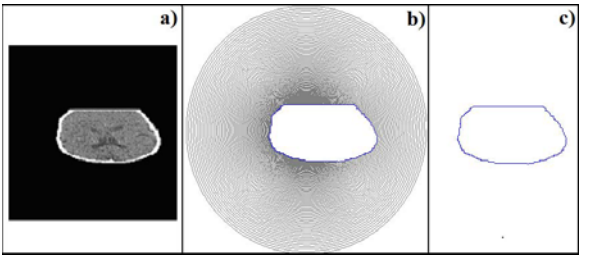

Fig. 1. (a) A CT section of brain; (b) The brain's boundary along with the curve defined by Eq(4) and evolved by Eq(3), to satisfy the condition given by Eq(5); (c) The extracted boundary alone

resolve this problem the model is "armed" with a re-parametrization approach [1,14,15,17]. To determine the direction of evolution after re-parametrization, the following concavity(convexity) equation is employed:

$$(x^{**} - x_i)(y^{*} - y^{**}) > (x^{*} - x^{**})(y^{**} - y_i). \tag{6}$$

In Eq(6) $P^{*} = (x^{*}(s^{*}, t^{*}), y^{*}(s^{*}, t^{*}))$ and $P^{**} = (x^{**}(s^{**}, t^{**}), y^{**}(s^{**}, t^{**}))$ are active contour points, which satisfy condition (5): $r(s^{*}, t^{*}) = r(s^{*}, t^{*} + \Delta t), r(s^{**}, t^{**}) = r(s^{**}, t^{**} + \Delta t)$, whereas (x_i, y_i) is a point added to the arc defined by P^{*} and P^{**} during the re-parametrization with Δs. If Eq(6) is satisfied the contour (the point x_i) evolves in the direction to the right side of the corresponding edge, if a clockwise walk along the contour is considered. See Figs 2(c), 3 (c) and 6(b) where the direction of evolution after the re-parametrization is shown with little parallel bars. Using the above concepts an algorithm was coded in Java and incorporated into the ACES module.

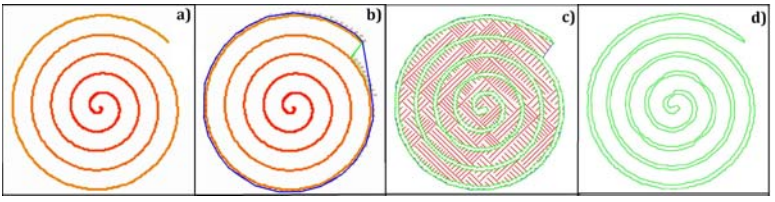

Fig. 2. (a) An image of a spiral; (b) The spiral along with the active contour which is re-parameterized and moved into the concavity; (c) The contour evolution into the spiral is shown by the straight segments; (d) spiral's contour

Observe that the ACES is always the first module to run and is halted in the vicinity of the object's boundary as shown in Figs 2(b), 3 (a) and 6(a). If the active contour is in about to converge into deep concavities a re-parametrization is performed with an arc segment Δs, given by the user. Then Eq(6) determines the right side (in case of clockwise traverse of the active contour) of every edge and the active contour evolves in the direction of this side by Eq(3) under condition given by Eq(5). The process of re-parametrization and evolution halts if the length of the arcs becomes smaller than Δs (Fig.2(c)).

As mentioned above the ACES module was tested with the spiral image shown in Fig 2(a). The image is of size 768x776. The software took 5.617 sec to extract the spiral's boundary using $\Delta s = 15$. The extracted boundary alone is shown in Fig 2(d).

3 Active Convex Hull Models on the Exact Solution

Paper[1] develops an ACHM applying the approximate solution of Eq(1). Normal and tangent forces were used to stop the contour evolution in this case. But the present section derives two new ACHM's on the base of the exact solution of

Eq(1). Instead of using forces a distance function or geometric line condition are employed in the present section.

Recall that the points on the initial contour are defined by Eq(4) for $t = 0.001$ and $s \in [0, 0.001155\frac{\pi}{a}]$. Define the function:

$$d(s,t) = |(x(s,0.001), y(s,0.001)) - (x(s,t), y(s,t))| \text{ for } t > 0.001 \qquad (7)$$

Theorem 1. *Given an object $\mathcal{O}$ in an image $f(x,y)$ and the center of the image belongs to $\mathcal{O}$. Also ε_1 and ε_2 are given for Eq.(5). Then the convex hull of $\mathcal{O}$ is defined by the active contour points $(x(s,t), y(s,t))$ which satisfy Eq.(5) and at which the function $d(s,t)$ has a local minimum, such that every triplet of consecutive minimums defines a convex up arc (this is an arc which satisfies the inverse of Eq(6)).*

Theorem 1 implies that the Exact Solution along with the Distance Minimums, which define convex up arcs, represent a new ACHM (ACHM-ESDM). Thus, the initial contour defined by Eq(4) is evolved by Eq(3) under condition (5) and is stoped in the proximity of the boundary (see Fig 3(a)). Then $d(s,t)$ is constructed using Eq(7) for t at which the contour was halted (Fig 3(a)). Next the local minimums of $d(s,t)$ are determined using the 1^{st} derivative test. Derivatives are approximated by finite differences on two consecutive nodes. To construct the convex hull Eq(6) is applied to determine the convexity of every triplet of consecutive points at which $d(s,t)$ has a local minimum. Triplets defining concavities are discarded.

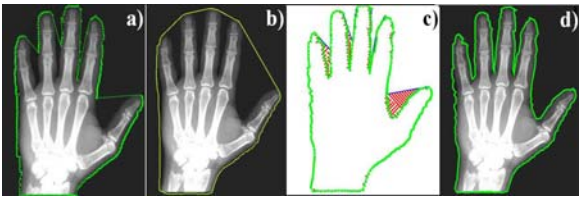

Fig. 3. (a) An X-ray of hand, the ACES in its vicinity; (b) The Convex hull of the hand; (c) The small bars show the direction of evolution after re-parameterizations. The hand's boundary; (d) The hand with the exact boundary.

The ACHM-ESDM is coded in Java, incorporated into the ACES software, and employed to extract the convex hull of the hand in Fig 3(a). The convex hull along with the hand is given in Fig 3(b). The next Fig 3(c) presents the direction of evolution and the hand's boundary after re-parameterizations.

It follows from Theorem-1 that the boundary points the active contour will meat first are the convex hull vertices. Consider now that for every convex object there is a unique circle to inscribe the object. Therefore the active contour points $(x_m, y_m), m = i, ..., j$ between every pair of convex hull vertices $P_i(x_i(s_i,t_i), y_i(s_i,t_i))$ and $P_j(x_j(s_j,t_j), y_j(s_j,t_j))$ belong to an *arc* of a circle.

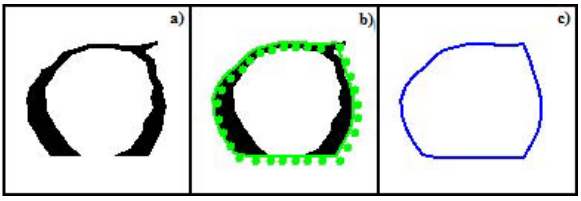

Fig. 4. (a) A section of a groundwater unit; (b) The section with its Convex Hull; (c) The convex hull alone

Thus to construct the convex hull every arc between convex hull vertices must evolve to a straight segment. A condition to stop arcs evolution on this segment is:

$$D_{ij} - (D_{im} + D_{mj}) = \pm\varepsilon_3, \tag{8}$$

where D_{ij}, D_{im} and D_{mj} are the Ecludian distances between the points P_i, P_j *and* P_m. The threshold ε_3 is chosen by the user.

The ACES model along with Eq(8) represents another convex hull model, called ACHM on the Exact Solution and Line Equation(ACHM-ESLE). The new model is incorporated into the ACES software. Experiments were performed with the ACHM-ESLE module using the images shown in Figs 4(a), 5(a). The convex hull of multiple objects is diven in Fig.5(b) whereas Fig 4(b) shows the convex hull of a single object defined in 0.047 seconds.

4 The Shell Algorithm with the ACES Model

The shell algorithm is designed in [1,14,15] to inscribe in a circle every object from an image, such that the center of the circle belongs to the object. The present section describes the shell algorithm in the light of the ACES model.

Consider an active contour which satisfies the initial condition formulated by Eq(4), evolves all the way to the image center, using Eq(3) and boundary condition (5). Then collect the points at which the contour hits or touches an object (finds discontinuities of f), and link every touching point with the center of the image or with another touch point (see Figs 5(c), 7(b)). The lines defined above are called tangent lines. The tangent lines along with the joint points P_j^m, between the active contour and object, form a shell. Two shells are defined in Fig 7 (b), eight in Fig 5(c). Three of them contain two objects whereas the remaining shells contain a single object.

In every shell m, for m $= [1, 2, ..., l]$ the mass center is calculated: $x_c^m = \frac{\sum_{j=1}^{k} x_j}{k+1}, y_c^m = \frac{\sum_{j=1}^{k} y_j}{k+1}$. Denote the mass center of shell m by $P_c^m = (x_c^m, y_c^m)$ and calculate

$$R^m = \max_{1 \le j \le k} \left\{ d(P_c^m, P_j^m), d(P_c^m, (\lfloor \frac{nc}{2} \rfloor, \lfloor \frac{nr}{2} \rfloor)) \right\} \tag{9}$$

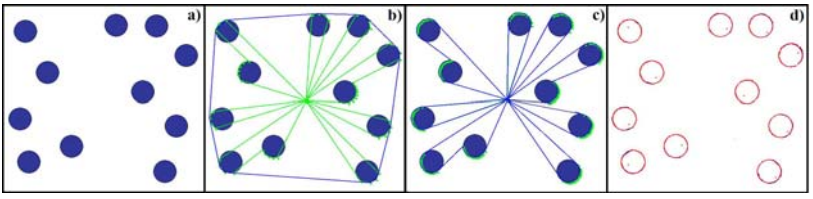

Fig. 5. (a) The original image; (b)The convex hull of the set of objects; (c) The shells of the objects; (d) The objects' boundaries

In Eq(9) "d" denotes the Euclidian distance between plane points, whereas $\left(\lfloor\frac{nc}{2}\rfloor, \lfloor\frac{nr}{2}\rfloor\right)$ denotes the center of the image. P_c^m and R_c^m are used by Eq(4) to define an initial contour which inscribes the objects from shell m. Again, the contour is evolved all the way to the center P_c^m. The process continues until a single object remains in every initial contour defined by Eq(4), and the center of this contour belongs to the object. The stop condition for the process is "No tangent line is built up after an evolution to the center".

From theoretical view point it is possible for the m^{th} initial contour to contain points not only from the m^{th} shell. To discard points cut from other shells the following approach is developed. Consider a point $P_k^m = (x_k^m, y_k^m)$ which satisfies Eqs(3) and (5) for a certain t. Therefore the following expression is derived from the discreet form of Eq(3) for $s = i_k$ and $t = j_k$: $(x_k^m, y_k^m) = \exp^{\left(i_k a - 4a^2 j_k\right)}[\cos\left(1000\sqrt{3}ai_k\right), \sin\left(1000\sqrt{3}ai_k\right)]$.

Denote by l_{m-1} and l_m the right and left most tangent lines which form the m^{th} shell. Denote by P_m the point at which l_m is a tangent to an object in the shell, and by P_{m-1} the point at which l_{m-1} is tangent to an object in the shell. Follows that both points satisfy the discrete form of Eqs(3) and (5) for $s = i_m$ and $t = j_m$, and for $s = i_{m-1}$ and $t = j_{m-1}$,

$$(x_m, y_m) = \exp^{\left(i_m a - 4a^2 j_m\right)}[\cos\left(1000\sqrt{3}ai_m\right), \sin\left(1000\sqrt{3}ai_m\right)]$$

$$(x_{m-1}, y_{m-1}) = \exp^{\left(i_{m-1} a - 4a^2 j_{m-1}\right)}[\cos\left(1000\sqrt{3}ai_{m-1}\right), \sin\left(1000\sqrt{3}ai_{m-1}\right)].$$

Now the following statement holds. The point P_k^m belongs to the m^{th} shell if and only if

$$i_{m-1} < i_k < i_m. \tag{10}$$

The Shells algorithm is linked to the ACES, ACHM-ESDM and ACHM-ESLE and all together they represent Integral Active Contour Model (IACM). To verify the shell module an experiment was performed with the image shown in Fig 5(a). The defined shells are given in Fig 5(c), while the objects' boundaries are shown in Fig 5(d).

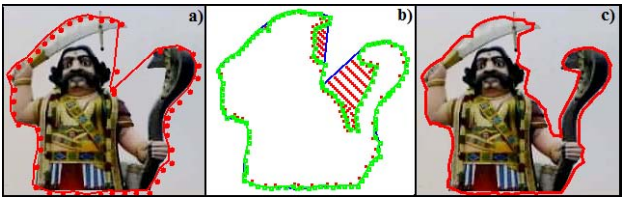

Fig. 6. (a) An image of Mahi's statue along with the IACM in the vicinity of the objects; (b) The directions of evolution and the boundary after re-parametrization; (c) The objects along with the extracted boundary

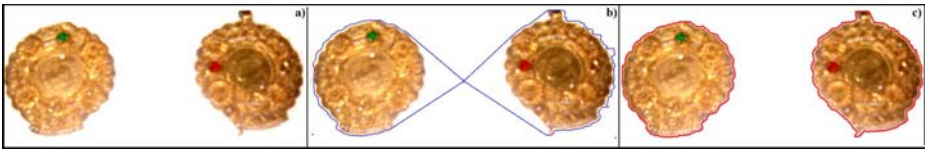

Fig. 7. (a) Image of crafts; (b) The crafts inscribed by two shells; (c) The crafts with the extracted boundary

5 Experimental Results

In the previous sections multiple models were developed and integrated as an IACM capable of extracting the boundaries, the convex hull and the concavities of multiple objects. To validate every module, experiments were performed across the previous sections. Thus, the Convex hull on Fig 3(b) was defined in 0.157 sec, whereas the hand boundary, shown in Fig 3(d), was extracted in 1.468 sec. The original image is of size 628x809.

The run time for defining the convex hull of the objects in the image of size 512x512 shown in Fig 5(b) is less than 10^{-4} sec. The shells in Fig 5(c) were determined in 1.62 sec, while the objects' boundaries shown in Fig 5(d) were extracted in 1.746 sec.

In the next experiment an image of Mahi's statue was used. The image is of size 210x200 and is shown in Fig 6(a). During the first stage of the work the ACES module set the contour in the vicinity of the boundary in less than 0.001 sec (Fig 6(a)). Next, a re-parametrization was performed and the directions of evolution were determined as shown in Fig 6(b). The extracted boundary of the objects is presented in Figs 6(b) and 6(c). The total elapsed time for the above work is 0.578 sec.

Another experiment was performed to extract the boundary of two crafts in an image of size 900x431, shown in Fig. 7 (a). The shell algorithm defined the two shells given in Fig 7(b) in 0.063 sec. Further the ACES and the re-parameterizations modules defined the boundary of every object shown in (Fig. 7 (c)). The total run-time for this job was 1.217 sec.

Table 1. Comparison of IACM, with VFC (R=N) [5] and GVF (N-iterations)[5,12]

Method	IACM	VFC	GVF
run in sec for 256x256	0.692	≈ 0.75	≈ 2
run in sec for 512x512	1.744	≈ 3	≈ 16

6 Discussion and Future Work

This paper presents an IACM and software capable of extracting convex hulls, boundaries and deep concavities of multiple objects. The IACM is composed of ACES, ACHM-ESDM, ACHM-ESLE, re-parametrization and shell algorithm and possess the following advantages:

- Automatic work with multiple objects, in an image, without user interaction;
- Very large capture range, because Eq(3) and (4) state that the intial contour may be set as far as the user wants (see Fig 1(b));
- Handles rectangular images, whereas [5, 12] report only square ones;
- Does not need stability convergence condition, while the active contours on differential equation do [1, 4, 8, 9, 17];
- Naturally extendable to the 3D case considering the 3D form of Eqs. (3-8);
- High accuracy of boundary and convex hull approximation because truncation error is generated only by the ACHM-ESDM. If the ACHM-ESLE is used truncation error is not generated at all. The accuracy also depends on the space step Δs (for s) and the time step Δt (for t), small Δs and Δt generate less error, but increase the run-time;
- Fewer operations and better runtime compare to VFC and GVF [5, 12] (see Table 1).

The later statement holds because the complexity of ACES, ACHM-ESDM, ACHM-ESLE depends on the number of pixels the Eqs(4), (6-8) are calculated on. Since the above listed models work with background pixels, whose number is less than N^2 (N-the longest side of an image) it follows that the complexity of each model included in IACM is $O(N^2)$.

The re-parametrization approach increases the number of background pixels used by Eqs (4) - (6), but this number could not exceed N^2. Thus the complexity of this approach is $O(N^2)$. The shell method splits the initial contour, inscribing the image and defined by Eq(4), to multiple contours. Each of them inscribes a single object. Therefore the complexity of the shell method does not exceed $O(N^2)$ as well. Follows that the complexity of the IACM is $O(N^2)$, which is favorable in comparison to VFC - $O(N^2 \log N)$ and GVF - $O(N^3)$ [5,12].

An elegant method which also applies re-parametrization but for the purpose of evolving "topology snakes" is represented in [17]. It uses a manual initialization of the curve and needs the correct choice of six parameters, whereas the present method is automatic.

A disadvantage of the IACM is its incapability to extract voids' boundaries (see Fig 6). Also, the user has to select the values for ε_1, ε_2, ε_3, Δs and Δt. Large values for Δs and Δt increase the speed but decrease the accuracy.

The future work continues with elaboration of Eq(3) and (5) to help the contour work with "low signal to noise ratio" [5] images. Also a work is under way to employ shells along with ACES model to determine voids. The IACM is to be extended to the 3D case.

References

1. Sirakov, N.M.: A New Active Convex Hull Model For Image Regions. Journal of Mathematical Imaging and Vision 26(3), 309–325 (2006)
2. Paragios, N., Deriche, R.: Geodesic, Active Regions and Level Set Methods for Supervised Texture Segmentation. Inter. Journal of Computer Vision, 223–247 (2002)
3. Rousson, M., Deriche, R.A.: Variational Framework for Active and Adaptive Segmentation of Vector Valued Images. In: Proc. IEEE Workshop Motion and Video Comp (December 2002)
4. Caselles, V., Kimmel, R., Sapiro, G.: Geodesic Active Contours. Inter. J of Computer Vision 22(1), 61–79 (1997)
5. Li, B., Acton, S.T.: Active Contour External Force Using Vector Field Convolution for Image Segmentation. IEEE Transactions On Image Processing 16(8), 2096–2106 (2007)
6. Kass, M., Witkin, A., Terzopoulos, D.: Snakes: Active Contour Models. Int'l J. Computer Vision 1(3), 211–221 (1987)
7. Kanaujia, A., Metaxas, D.N.: Large Scale Learning of Active Shape Models. In: Proc. IEEE ICIP2007, San Antonio, September 2000, p I-265-268 (2007) ISBN: 1-4244-1437-7
8. Chan, T., Shen, J., Vese, L.: Variational PDE Models in Image Processing. Notices American Math Society 50(1), 14–26 (2003)
9. Sapiro, G.: Geometric Partial Differential Equation and Image Processing. Cambridge Univ. Press, Cambridge (2001)
10. Osher, S., Sethian, J.A.: Fronts Propagating with Curvature Dependent Speed: Algorithms Based on Hamilton-Jacobi Formulations. Journal of Computational Physics 79, 12–49 (1988)
11. Sethian, J.A.: A fast marching level set method for monotonically advancing fronts. Applied Mathematics 93(02-96), 1591–1595 (1996)
12. Xu, C., Prince, J.L.: Gradient Vector Flow Deformable Models. In: Bankman, I. (ed.) Handbook of Medical Imaging, pp. 159–169. Academic Press, London (2000)
13. Grenander, U., Miller, M.I.: Pattern Theory: From Representation to Inference. Oxford University Press, Oxford (2007)
14. Sirakov, N.M.: Monotonic Vector Forces and Green's Theorem For Automatic Area Calculation. In: Proc. IEEE ICIP 2007, San Antonio, September 2007, vol. IV, pp. 297–300 (2007) ISBN: 1-4244-1437-7
15. Sirakov, N.M.: Automatic Concavity's Area Calculation Using Active Contours and Increasing Flow. In: Proc. of ICIP 2006, Atlanta, October 2006, pp. 225–228 (2006) ISBN: 1-4244-0481-9
16. Sirakov, N.M., Simonelli, I.: A New Automatic Concavities Extraction Model. In: Proc of Southwest Sym. on Image Analysis and Inter., pp. 178–182. IEEE Computer Society, Denver (2006)
17. McInerney, T., Terzopolous, D.: T-Snakes: Topology adaptive snakes, Medical image analysis, vol. 4, pp. 73–91. Elsevier Science B.V., Amsterdam (2000)